Exploiting Optical Asymmetry for Controlled Guiding of Particles with Light

Ognjen Ilic,*,† Ido Kaminer,† Yoav Lahini,† Hrvoje Buljan,‡ and Marin Soljačić†

Department of Physics, Massachusetts Institute of Technology, Cambridge, MA 02139, United States, and Department of Physics, University of Zagreb, 10000 Zagreb, Croatia

Received January 10, 2016; E-mail: ilico@mit.edu

Abstract:

Conventional methods of manipulating particles with light, such as optical tweezers and optical tractor beams, rely on beam-shaping to realize complex electromagnetic field profiles and are thus sensitive to scattering. Here, we show that by introducing tailored optical asymmetry in the particle, we can realize a novel guiding method that is controllable by the frequency of light, without regard to the direction or the shape of the light beam. With detailed stochastic simulations, we demonstrate guiding of a two-faced nanoparticle where the optically induced thermophoretic drift serves as the propulsion mechanism. Exploiting the difference in resonant absorption spectra of the two materials, we create a bidirectional local thermal gradient that is externally switchable. This is advantageous because the frequency of a light beam, unlike its shape or coherence, is preserved even in strongly scattering environments. Since this approach is insensitive to scattering and applicable to many particles at once as well as particles that cannot be optically resolved, it may enable useful applications in biology, microfluidics, in vivo tasks, and colloidal science.

Controlling the motion of nano- and microscale particles and objects has been a long-sought goal in science and engineering.[1] These functional particles—also referred to as microrobots, microswimmers and nanomotors—carry the potential for a wide range of applications across a variety of disciplines, including biology, medicine, microfluidics, colloidal science and many others.[2] Thus far, external control of the position of such particles has been possible by methods that rely on chemical,[3] electric,[4] magnetic,[5] acoustic,[6] and temperature[7–9] effects to power the transport on the nano and the microscales. However, many of the proposed schemes fail to meet the conditions for optimal particle guiding, which include controllable and high-speed movement, and biocompatibility as well as the ability to operate in biologically relevant environments.[10]

Light has also been used to transport and guide wavelength and subwavelength sized particles in schemes that include optical tweezers[11–15] and optical tractor beams.[16,17] However, these approaches require focusing and shaping of the light beam and are thus particularly sensitive to scattering. Light-induced thermal effects can exert force on a particle: for example, in a metal-dielectric particle (such as a Janus particle[18]), the heat generated by the absorption of light in the metal side induces a local temperature difference, resulting in propulsion (thermophoresis) along the axis of the temperature gradient.[7,8,19–26] Because the thermophoretic drift is based on absorption of light, it is robust to scattering in the surrounding environment. However, this same feature is also a disadvantage: as the induced drift always points in the same direction, it is difficult to guide (steer) an object to the desired location. Currently, the only way to achieve a level of particle control is by switching on the thermophoretic action whenever the particle orientation is facing the target and off when it is not.[22,23] This requires real-time optical imaging of the particle position and orientation and is limited to particles large enough to be optically resolved, imposing limitations on thermophoretic guiding. It would be desirable to develop a guiding method that eliminates such restrictions, while maintaining the robustness of the thermophoretic force.

Here, we achieve this with a new type of asymmetric particle, and show that such a particle can be transported in space by only switching the incident beam's frequency (this can, for example, be done by using two different monochromatic sources). We demonstrate this concept—which does not require focusing or manipulation of the light beam—on a particle with two counter faces (e.g. Figure 1). The two faces (in our case, gold and titanium-nitride) are designed to preferentially absorb light of different wavelength (500 and 800 nm in our case) regardless of the particle orientation, thus allowing for bidirectional motion. As an example, a guiding scheme that relies on a particle position (or distance to the target) can be used to transport a nano particle over distances greater than 100μm (see Figure 5 and, also, Supporting Information, Video). Because the scheme relies only on the particle location or distance to the target (and not its orientation[22,23]), the proposed method can be used to guide subwavelength particles that are too small to be fully optically resolved or particles that cannot be visualized at all. Eliminating the need for focusing or shaping of the light beam, multiple particles or particles in strongly scattering environments can be guided. Finally, owing to biocompatibility and nontoxicity of light, this approach to particle guiding may find biological and in-vivo applications.

We begin by examining a plane, linearly-polarized, incident light wave of the form $\mathbf{E}_{\mathrm{inc}} = \hat{x}E_0\exp(ik_0 z - i\omega t)$ impinging on a composite asymmetric particle, as shown in Figure 1a. Because the particle is roughly spherical, its motion can be approximated by a set of differential equations for translation and rotation:[27–29]

$$m\frac{\mathrm{d}^2\mathbf{x}}{\mathrm{d}t^2} = \mathbf{F}_{\mathrm{opt}}(\mathbf{P}) + \frac{1}{\mu}\mathbf{U}_{\mathrm{th}}(\mathbf{P}) - c_t\frac{\mathrm{d}\mathbf{x}}{\mathrm{d}t} + \sigma_t\xi(t) \qquad (1)$$

$$I\frac{\mathrm{d}\boldsymbol{\omega}}{\mathrm{d}t} = \mathbf{M}_{\mathrm{opt}}(\mathbf{P}) - c_{rot}\boldsymbol{\omega} + \sigma_{rot}\zeta(t) \qquad (2)$$

where $\mathbf{x}$ is the position of the particle, $\boldsymbol{\omega}$ its angular velocity and m and I are the particle mass and the moment of inertia, respectively. The particle mobility μ relates to the viscous drag through $1/\mu = c_t = 6\pi\eta R$; similarly, for rotation $c_{rot} = 8\pi\eta R^3$, where R is the particle radius and η is the viscosity

†Massachusetts Institute of Technology

‡University of Zagreb

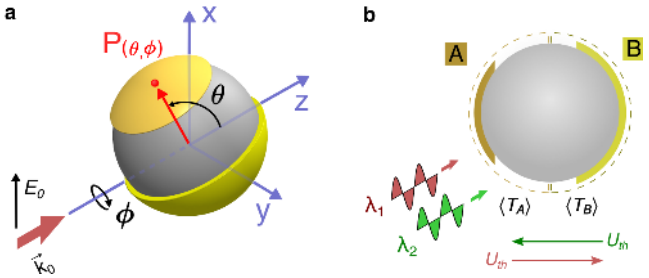

Figure 1. Light beam impinges on an asymmetric particle consisting of a uniform dielectric core and two opposing caps, labeled A and B. The caps are made of materials that allow for selective light absorption based on the wavelength of the incident beam (λ_1, red; λ_2, green). As a result, the direction of the temperature gradient ($\langle T_A\rangle - \langle T_B\rangle$) is wavelength-dependent. The optically induced thermophoretic drift $\mathbf{U}_{\rm th}$, proportional to the temperature gradient, can be used to transport the particle in space (the guiding scheme is illustrated in Figure 4). (a) 3D view and (b) cross-section of a polystyrene particle with a titanium-nitride (A) and gold (B) cap.

of the medium.[30] In our case, the ambient medium is water, with $\eta = 8.9 \times 10^{-4}$Pa s.[31] The diffusion in the system is characterized by the Langevin stochastic terms (ξ, ζ), where $\sigma_t = \sqrt{2k_bTc_t/m}$ and $\sigma_{rot} = \sqrt{2k_bTc_{rot}/I}$ and $\xi(t)$ is a set of independent Gaussian variables with zero mean and covariance $\langle \xi_i(t)\xi_j(t')\rangle = \delta_{ij}\delta(t-t')$ (the same is true for $\zeta(t)$). Finally, the orientation of the particle (which is fixed in the frame of the particle) is coupled to its angular velocity through $\mathrm{d}\mathbf{P}(t)/\mathrm{d}t = \boldsymbol{\omega}(\mathbf{P},t)\times\mathbf{P}(t)$. This, together with eqs 1 and 2, can be used to evolve the position and orientation of the particle in time. We remark that these equations are valid for laminar flows[30] (where the expressions for the translational and rotational viscous drags are applicable).

In the equations of motion above, the key term for particle guiding is the self-induced thermophoretic drift $\mathbf{U}_{\rm th}$. This drift depends on the particle orientation $\mathbf{P}$. Thus, we explore all possible directions that the particle can be facing in with respect to the incident light beam: these are given by the angle that the apex of the cap A (point $\mathbf{P}$) makes relative to the coordinate system. Angles θ, ϕ correspond to the polar (with respect to $\hat{z}$) and the azimuthal angle, respectively (Figure 1). We obtain the scattered electromagnetic fields (without any approximations) using a finite-element-method solver (Comsol Multiphysics) and subsequently calculate (also in Comsol) the steady-state temperature distribution in the system. For the heat transfer simulation, the absorbed electromagnetic power in the caps A and B serves as the heat source. From the equilibrium temperature distributions we evaluate the average surface temperatures, $\langle T_A\rangle$ and $\langle T_B\rangle$, that correspond to the hemispheres that contain caps A and B, respectively (dashed half-circles in Figure 1b).

As previously mentioned, the thermophoretic drift $\mathbf{U}_{\rm th}$ that the particle experiences is directly proportional to the optically-induced temperature gradient. While the magnitude of the thermophoretic drift scales linearly with the intensity of the actuating light, we control the sign of $\mathbf{U}_{\rm th}$ by switching the beam frequency/wavelength. To demonstrate this behavior, we select gold and titanium-nitride (TiN) as the two materials that make the cap B and the cap A, respectively. The choice of these two materials is predicated on their relative resonant absorption strengths of light of different wavelength. Our choice is partly motivated by examining how a uniform spherical particle absorbs light. Figure 2 shows the absorption efficiency $Q_{\rm abs}$ as a function of wavelength and size for homogeneous gold and titanium-nitride spherical particles (the absorption efficiency is calculated from Mie scattering equations). We observe a clear difference in the optimal wavelength ranges for absorption in the two materials and exploit this feature in our design. Specifically, we focus on two wavelengths, 800 and 500 nm (shown as a red/green line).

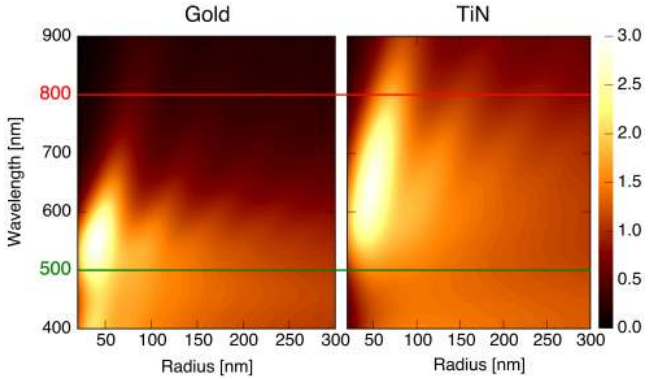

Figure 2. Absorption efficiency as a function of wavelength and radius for a homogeneous gold (left) and titanium-nitride (right) spherical particle, in water. Values obtained from Mie scattering equations. Highlighted green (500 nm) and red (800 nm) lines correspond to the two wavelengths used for selective heating of the two hemispheres of the composite asymmetric particle (Figure 1a).

As the scattering of light by a cap-like particle can be quite different from the scattering of a uniform sphere, Figure 2 is used primarily as a guide. It suggests that, for 800 nm light, the gold side should not heat substantially. Because TiN appears to have a broader spectral absorption range, it further suggests that the corresponding TiN cap (in the composite particle) should be made smaller than the gold cap. This would ensure that for 500 nm light the hemisphere with the gold cap would get hotter, no matter the orientation of the particle with respect to the incoming light. Given the choice of materials for the core particle (polystyrene) and the two caps (gold and TiN), the geometry of the composite particle is further optimized to achieve such behavior. With the size of the particle (diameter $a = 1\mu$m) and the caps' thickness (60 nm) fixed (see Supporting Information), the relative sizes of the two caps are chosen such that, no matter the orientation of the particle with respect to the incident beam, the frequency of the beam solely determines which of the two half-surfaces is hotter.

Figure 3 further elucidates this: it shows the equilibrium temperature difference (normalized to the incident beam power) for the two wavelengths (800 nm in (a) and 500 nm in (b)) for all possible orientations ($\theta = 0 - 180°, \phi = 0 - 360°$). To achieve the desired behavior, the chosen size of the gold(TiN) cap corresponds to the spherical angle of $6\pi/5(2\pi/5)$, as shown in the cross-sectional view in Figure 1b. Temperature $T_{\rm Au}$ corresponds to the average surface temperature of the hemisphere that contains the gold cap (corresponding to the dashed half-circle B in Figure 1b); the same applies for $T_{\rm TiN}$. When the wavelength of the incident beam of light is 800 nm (Figure 3a), the temperature of the side with the TiN cap is always higher than the temperature of the side with the gold cap, no matter the orientation of the particle. When the TiN cap faces toward the incoming 800 nm beam (i.e. $\theta = 180°$, top sketch on the right in Figure 3a), it is reasonable to expect that the TiN side

will absorb more and reach a higher temperature. However, even when the gold cap directly faces the incoming beam (i.e. $\theta = 0°$, bottom sketch on the right in Figure 3a), the TiN side is still hotter when λ=800 nm. For λ=500 nm the opposite is true: the hemisphere with the gold cap will be hotter no matter the orientation of the particle. If the two caps were the same size (had the same area coverage), this would no longer be the case (Supporting Information, Figure 1). We remark that the literature values for the permittivity, density, heat capacity and thermal conductivity for gold,[31,32] titanium nitride,[33,34] polystyrene,[35] and water[31] are used in the finite element simulation for the heat equation. The orientation of the particle is uniquely determined by angles θ, ϕ (Figure 1a; the direction of the beam is fixed $\mathbf{k} = k_0\hat{z}$); in numerical simulations, we calculate the temperature gradient for all possible values of θ, ϕ in steps of 5°. For orientations corresponding to intermediate angles, the temperature gradient is obtained by bilinear interpolation. In the Supporting Information, we analyze the sensitivity of the composite particle design to variations in geometrical parameters (as well as cap corners) and find that small deviations would introduce no qualitative change in the heating patterns. Finally, in our model, we assume that all parameters (such as the permittivity, heat conductivity, etc.) are temperature-independent in the relevant temperature range. When this is the case, the Maxwell's equations and the heat equation are linear, and the induced temperature difference (between the hot hemisphere and the cold hemisphere) is directly proportional to the source intensity. Our simulations for different incident source intensities confirm this behavior (for arbitrary particle orientation). Hence, the calculated quantities are reported normalized to the beam intensity. We note that for strong enough light intensities, the intense local heating can alter the particle's environment, including viscosity and the thermophoretic mobility.[36,37] However, for the source intensities we use here, we do not expect qualitative changes in our results.

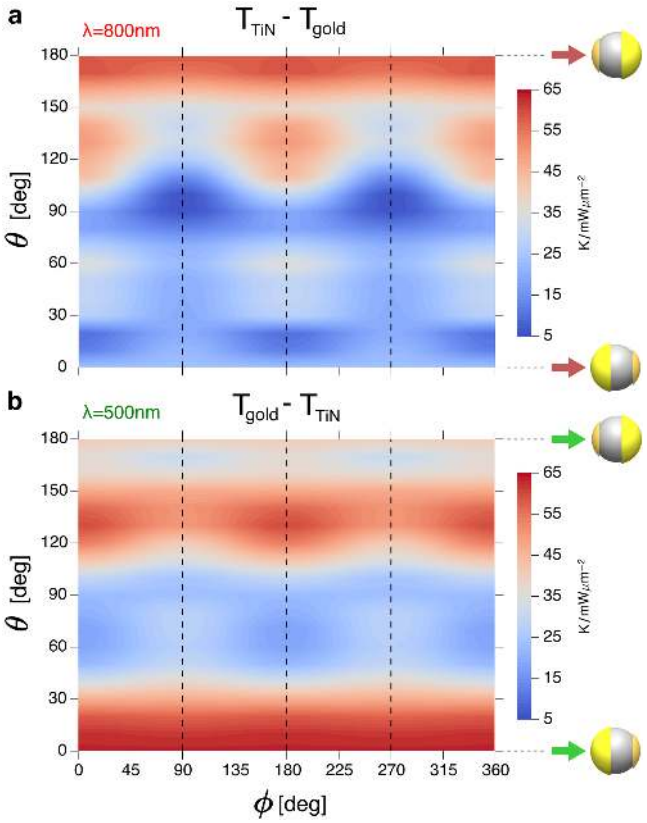

Figure 3. Difference in the average surface temperature of the hemisphere that contains the TiN cap and the hemisphere that contains the gold gap (Figure 1) for all particle orientations (θ, ϕ). When the incident light is 800 nm (**a**) the TiN hemisphere is always hotter, even when the gold side directly faces the incident light ($\theta = 0°$). For 500 nm light (**b**), the opposite is true: the hemisphere with the gold cap is always hotter. The four sketches show the two wavelengths of light (red and green arrows indicate the incoming direction of the light) in the two special orientations $(\theta = 0°, 180°)$.

This asymmetric absorption of light at different wavelengths results in a tunable, bidirectional, thermophoretic drift. In general, the thermophoretic drift is directly proportional to the temperature gradient

$$\mathbf{U}_{\rm th} = -D_T \nabla T \tag{3}$$

where D_T is the thermal diffusion coefficient. The thermal diffusion coefficient (also known as the thermophoretic mobility coefficient) is a complex quantity that may be affected by the particle size, material, the composition of the ambient medium, and so on.[38,39] For thermophoresis in fluids, the value of D_T is commonly inferred from experiments. The gradient in the temperature in eq 3 can be related to the induced temperature difference across the particle.[8] For the purposes of numerically iterating eqs 1 and 2, we write $\mathbf{U}_{\rm th}/\mu = -c_{\rm th}\left[\langle T_{\rm TiN}\rangle - \langle T_{\rm Au}\rangle\right]\hat{\mathbf{P}}$, where $\langle T_{\rm Au}\rangle$ is the average surface temperature on the hemisphere that contains the gold cap (likewise for the TiN cap), $\hat{\mathbf{P}}$ is the unit-vector pointing from the center of the gold cap to the center of the TiN cap (Figure 1a) and $c_{\rm th}$ is the proportionality factor. In order to estimate the magnitude of the proportionality coefficient $c_{\rm th}$ that relates the thermophoretic drift to the difference in the average surface temperatures of the two sides, we refer to references 22 and 23. There, from experimental data for a single-capped particle of similar dimensions to that of Figure 1 ($a = 1\mu$m polystyrene particle with a 60 nm gold cap), the authors provide an estimate for the relationship between the actuating laser intensity, thermophoretic drift and the induced temperature difference. On the other hand, from our finite-element simulations (for the particle of the same size), we relate the source intensity to the temperature distribution, averaged over all particle orientations. Combining these, we estimate the proportionality constant of $c_{\rm th} \sim 0.01\frac{\rm pN}{\rm K}$, which is used for numerically evolving eqs. 1 and 2.

Evolving the stochastic equations of translation and rotation, we show how the bidirectional thermophoretic drift can efficiently propel such an asymmetric particle. Figure 4 illustrates the guiding scheme. In a time interval τ_1 the particle is driven from A to B due to the induced temperature difference (as well as translational diffusion). Going forward, we present two guiding algorithms, corresponding to different experimental scenarios. First, when the location of the particle is observed (i.e. points A and B, as in Figure 4a), the guiding scheme is as follows: (case 1) if the direction to target (BT) is within the forward cone (angle ψ around AB), then the light of the same wavelength should be used for the next interval τ_1; (case 2) if the direction to target (BT) is within the backward cone (of the same angle ψ) then the wavelength should be switched (from 500 to 800 nm, or vice versa); finally, if neither is true (case 3), no light is used for the time interval τ_2 allowing for rotational diffusion to reorient the particle. The scheme is repeated until the particle is deemed to have reached the target; in our case, the

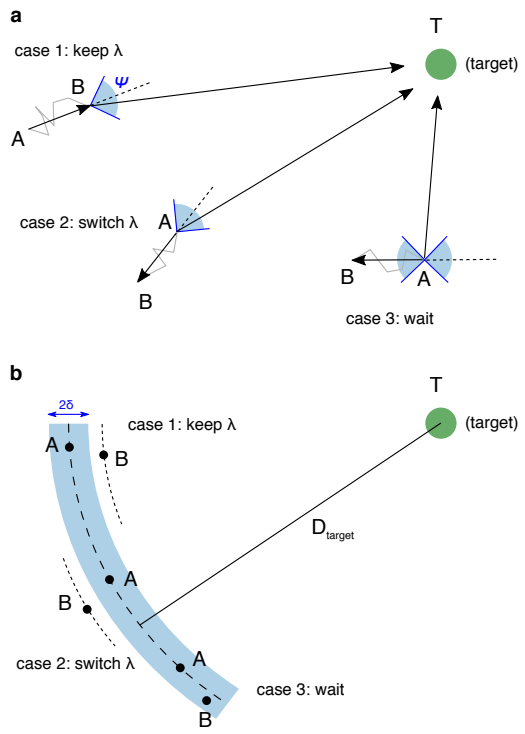

Figure 4. Scheme for guiding the composite asymmetric particle: the particle, that in the short time interval τ_1 moves from A to B, can be guided to the target location (T) either when its location is known (**a**) or when only the distance to the target is known (**b**).

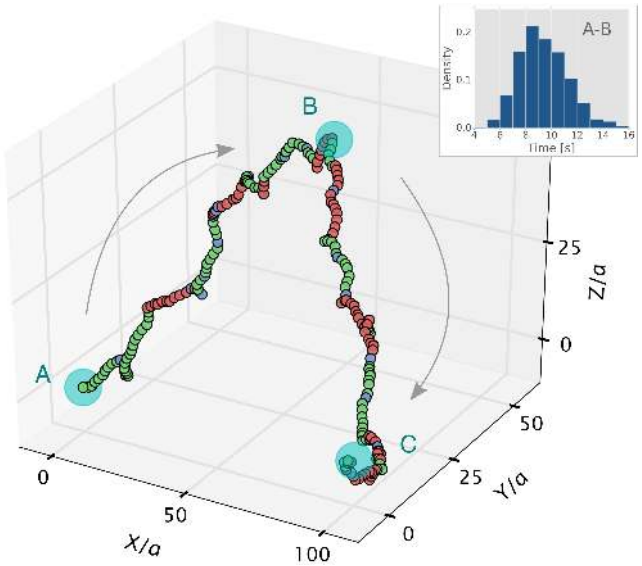

Figure 5. Example of a composite asymmetric particle (a=1μm, Figure 1) transported along the target A-B-C route, by switching the wavelength of the actuating light: 800 nm (red circles) and 500 nm (green circles). At times, the heating is temporarily turned off to allow for rotational diffusion to reorient the particle (blue circles). Inset: histogram of the time required to transport such a particle from A to B (N=10^3 runs). See Supporting Information, Video.

criterion for stopping is when the particle is within 10μm of the target (we used the admittance cone corresponding to $\cos(2\psi) = 0.3$).

However, the particle does not need to be visualized at all for the guiding scheme to work (Figure 4b). When just the distance to the target (D_{target}) is known, the guiding scheme is similar: (case 1) if in the time interval τ_1 the particle moves at least a distance δ closer to target, the same wavelength should be repeated; (case 2) if it moves more than δ further away from the target, the wavelength should be switched; finally, if the particle remains within a distance δ (case 3, shaded blue region in Figure 4b), the algorithm waits τ_2. Here, the actual locations of the particle (A and B) are never known (hence, the trajectories AB are not labeled in the figure).

Figure 5 shows an example trajectory of a particle guided along the arbitrary target route A-B-C (see Supporting Information, Video). For this particular case, the location is recorded every τ_1 =20 ms (e.g. from a 50 fps tracking camera), and the "wait" period is τ_2 =50 ms. The red circles correspond to the intervals when the 800 nm light is used; similarly, the green circles correspond to 500 nm light. The intensity of the light source in both cases is I_0 =1 mW/μm^2. Finally, the blue circles indicate the time intervals where the algorithm chose to turn off heating and wait (τ_2). In N=10^3 of such simulations, the particle always reached its target destination; the average time for the A-B portion (of length 50a$\sqrt{3}$) was 9.4 s, with the standard deviation of 1.9 s (see inset in Figure 5). The parameters for this set of simulations ($I_0, \tau_1, \tau_2, \psi$) are examples to showcase the feasibility of our particle transport scheme; however, the particle can be guided for a wide range of parameters. In the Supporting Information, we explore a range of parameter values and quantify the conditions for this approach to localize a particle to a specific point in space. For an appropriate combination of source intensity and guiding time step, the average distance can be similar to the size of the particle (Supporting Information, Figure 3), thus, allowing for an accurate approach to the target. The fundamental limitation of this type of guiding comes from the rotational diffusion time, $\tau_{rot} = 1/2D_{rot} \approx 0.34$ s for a 1 μm particle in water. This sets the upper bound for the actuation time interval in the guiding scheme $\tau_1 \leq \tau_{rot}$, to ensure the orientation of the particle does not become completely randomized. Since $\tau_{rot} \sim R^3\eta$, it implies that larger particles (or particles in more viscous surroundings) can be guided using slower tracking (longer τ_1). Naturally, more sophisticated guiding algorithms that leverage the combination of the beam intensity, particle's velocity and trajectory history can be developed on top of the basic idea presented here.

As previously mentioned, an important feature of our guiding scheme is that it also works when just the distance to the target is known. This is particularly useful for particles that cannot be visualized, and the distance to the target is instead inferred by other means (i.e. a chemical/biological signal that is proportional to the particle-target separation). For this approach (Figure 4b), the average time for the A-B segment in Figure 5 is 10.7 s and the standard deviation is 2.5 s (for a total of 10^3 runs; the particle reached the target every time). Finally, this approach is not limited to single particles: the bidirectional nature of the proposed guiding mechanism could be used to move a collection of such asymmetric particles, also using only two different source wavelengths. The details of this scheme can be found in the

Supporting Information.

In summary, here we proposed a novel method of particle guiding with light that leverages optical asymmetry to achieve targeted control of particle position. It relies on a new type of asymmetric particle, with opposing faces made of different materials that allow for bidirectional, light-induced, thermophoretic drift. As an example, we presented a design of a particle with a gold face and a titanium-nitride face that can be pushed in opposing directions based solely on the frequency of light. This offers robustness, as the light beam frequency, unlike its shape or coherence, is preserved even in strongly scattering media. Stochastic simulations based on common experimental parameters confirm that such a particle could be efficiently guided, without regard to the direction of the light source. Moreover, the particle to be transported does not need to be visualized at all. The parameters in our proposed optical guiding scheme, specifically the materials and the wavelengths, are chosen to demonstrate the proof of concept and are in no way ideal. An exciting direction for future studies would be to design similar optical asymmetry in the wavelength spectra associated with increased organ and tissue transparency,[40,41] an important step toward enabling biological and in vivo applications.

This work was partially supported by the Army Research Office through the ISN under Contract No. W911NF-13-D-0001, and by the MRSEC Program of the NSF Under Award No. DMR-1419807. The research of I.K. was also partially supported by the Seventh Framework Programme of the European Research Council (FP7Marie Curie IOF) under grant agreement no. 328853MCBSiCS. HB acknowledges support from the QuantiXLie Center of Excellence.

References

(1) Whitesides, G. M. The once and future nanomachine. *Sci. Am.* **2001**, *285*, 70–75.
(2) Mallouk, T. E.; Sen, A. Powering Nanorobots. *Sci. Am.* **2009**, *300*, 72–77.
(3) Mano, N.; Heller, A. Bioelectrochemical Propulsion. *J. Am. Chem. Soc.* **2005**, *127*, 11574–11575.
(4) Fan, D. L.; Zhu, F. Q.; Cammarata, R. C.; Chien, C. L. Controllable High-Speed Rotation of Nanowires. *Phys. Rev. Lett.* **2005**, *94*.
(5) Dreyfus, R.; Baudry, J.; Roper, M. L.; Fermigier, M.; Stone, H. A.; Bibette, J. Microscopic artificial swimmers. *Nature* **2005**, *437*, 862–865.
(6) Wang, W.; Castro, L. A.; Hoyos, M.; Mallouk, T. E. Autonomous Motion of Metallic Microrods Propelled by Ultrasound. *ACS Nano* **2012**, *6*, 6122–6132.
(7) Paxton, W. F.; Sen, A.; Mallouk, T. E. Motility of Catalytic Nanoparticles through Self-Generated Forces. *Chem. - Eur. J.* **2005**, *11*, 6462–6470.
(8) Jiang, H.-R.; Yoshinaga, N.; Sano, M. Active Motion of a Janus Particle by Self-Thermophoresis in a Defocused Laser Beam. *Phys. Rev. Lett.* **2010**, *105*.
(9) Baraban, L.; Streubel, R.; Makarov, D.; Han, L.; Karnaushenko, D.; Schmidt, O. G.; Cuniberti, G. Fuel-Free Locomotion of Janus Motors: Magnetically Induced Thermophoresis. *ACS Nano* **2013**, *7*, 1360–1367.
(10) Rao, K. J.; Li, F.; Meng, L.; Zheng, H.; Cai, F.; Wang, W. A Force to Be Reckoned With: A Review of Synthetic Microswimmers Powered by Ultrasound. *Small* **2015**, *11*, 2836–2846.
(11) Ashkin, A. Acceleration and Trapping of Particles by Radiation Pressure. *Phys. Rev. Lett.* **1970**, *24*, 156–159.
(12) Ashkin, A. Optical Levitation by Radiation Pressure. *Appl. Phys. Lett.* **1971**, *19*, 283.
(13) Grier, D. G. A revolution in optical manipulation. *Nature* **2003**, *424*, 810–816.
(14) Juan, M. L.; Righini, M.; Quidant, R. Plasmon nano-optical tweezers. *Nat. Photonics* **2011**, *5*, 349–356.
(15) Wang, K.; Schonbrun, E.; Steinvurzel, P.; Crozier, K. B. Trapping and rotating nanoparticles using a plasmonic nano-tweezer with an integrated heat sink. *Nat. Commun.* **2011**, *2*, 469.
(16) Chen, J.; Ng, J.; Lin, Z.; Chan, C. T. Optical pulling force. *Nat. Photonics* **2011**, *5*, 531–534.
(17) Shvedov, V.; Davoyan, A. R.; Hnatovsky, C.; Engheta, N.; Krolikowski, W. A long-range polarization-controlled optical tractor beam. *Nat. Photonics* **2014**, *8*, 846–850.
(18) Walther, A.; Müller, A. H. E. Janus Particles: Synthesis, Self-Assembly, Physical Properties, and Applications. *Chem. Rev.* **2013**, *113*, 5194–5261.
(19) Piazza, R. Thermal forces: colloids in temperature gradients. *J. Phys.: Condens. Matter* **2004**, *16*, S4195–S4211.
(20) Golestanian, R.; Liverpool, T. B.; Ajdari, A. Designing phoretic micro- and nano-swimmers. *New J. Phys.* **2007**, *9*, 126–126.
(21) Bickel, T.; Majee, A.; Würger, A. Flow pattern in the vicinity of self-propelling hot Janus particles. *Phys. Rev. E* **2013**, *88*.
(22) Qian, B.; Montiel, D.; Bregulla, A.; Cichos, F.; Yang, H. Harnessing thermal fluctuations for purposeful activities: the manipulation of single micro-swimmers by adaptive photon nudging. *Chem. Sci.* **2013**, *4*, 1420.
(23) Bregulla, A. P.; Yang, H.; Cichos, F. Stochastic Localization of Microswimmers by Photon Nudging. *ACS Nano* **2014**, *8*, 6542–6550.
(24) Nedev, S.; Carretero-Palacios, S.; Kühler, P.; Lohmüller, T.; Urban, A. S.; Anderson, L. J. E.; Feldmann, J. An Optically Controlled Microscale Elevator Using Plasmonic Janus Particles. *ACS Photonics* **2015**, *2*, 491–496.
(25) Lamhot, Y.; Barak, A.; Rotschild, C.; Segev, M.; Saraf, M.; Lifshitz, E.; Marmur, A.; El-Ganainy, R.; Christodoulides, D. N. Optical Control of Thermocapillary Effects in Complex Nanofluids. *Phys. Rev. Lett.* **2009**, *103*.
(26) Lamhot, Y.; Barak, A.; Peleg, O.; Segev, M. Self-Trapping of Optical Beams through Thermophoresis. *Phys. Rev. Lett.* **2010**, *105*.
(27) Lemons, D. S.; Anthony, G. Paul Langevin's 1908 paper "On the Theory of Brownian Motion" ["Sur la théorie du mouvement brownien," C. R. Acad. Sci. (Paris) 146, 530-533 (1908)]. *Am. J. Phys.* **1997**, *65*, 1079.
(28) Lewis, J.; McConnell, J.; Scaife, B. The rotational Brownian motion of a sphere. *Phys. Lett. A* **1974**, *49*, 303–305.
(29) Coffey, W.; Kalmykov, Y.; Waldron, J. *The Langevin Equation: With Applications in Physics, Chemistry, and Electrical Engineering*; Series in Contemporary Chemical Physics; World Scientific, 1996.
(30) Lamb, H. *Hydrodynamics*; Dover, New York, 1945.
(31) Haynes, W. In *CRC Handbook of Chemistry and Physics*, 92nd ed.; Haynes, W., Ed.; CRC Press / Taylor and Francis Group, LLC, Boca Raton, FL, 2012.
(32) Johnson, P. B.; Christy, R. W. Optical Constants of the Noble Metals. *Phys. Rev. B* **1972**, *6*, 4370–4379.
(33) Guler, U.; Ndukaife, J. C.; Naik, G. V.; Nnanna, A. G. A.; Kildishev, A. V.; Shalaev, V. M.; Boltasseva, A. Local Heating with Lithographically Fabricated Plasmonic Titanium Nitride Nanoparticles. *Nano Lett.* **2013**, *13*, 6078–6083.
(34) Pierson, H. O. *Handbok of refractory carbides and nitrides: properties, characteristics, processing, and applications*; Noyes Publications, Park Ridge, N.J., 1996.
(35) Marcus, S.; Blaine, R. Thermal conductivity of polymers, glasses and ceramics by modulated DSC. *Thermochim. Acta* **1994**, *243*, 231–239.
(36) Duhr, S.; Braun, D. Why molecules move along a temperature gradient. *Proc. Natl. Acad. Sci.* **2006**, *103*, 19678–19682.
(37) Rings, D.; Selmke, M.; Cichos, F.; Kroy, K. Theory of Hot Brownian Motion. *Soft Matter* **2011**, *7*, 3441.
(38) Putnam, S. A.; Cahill, D. G.; Wong, G. C. L. Temperature Dependence of Thermodiffusion in Aqueous Suspensions of Charged Nanoparticles. *Langmuir* **2007**, *23*, 9221–9228.
(39) Braibanti, M.; Vigolo, D.; Piazza, R. Does Thermophoretic Mobility Depend on Particle Size? *Phys. Rev. Lett.* **2008**, *100*.
(40) Byrnes, K. R.; Waynant, R. W.; Ilev, I. K.; Wu, X.; Barna, L.; Smith, K.; Heckert, R.; Gerst, H.; Anders, J. J. Light promotes regeneration and functional recovery and alters the immune response after spinal cord injury. *Lasers Surg. Med.* **2005**, *36*, 171–185.
(41) Hamblin, M. R.; Huang, Y.-Y. *Handbook of photomedicine*; Boca Raton : CRC Press, 2013., 2013.

Graphical TOC Entry